

Multi-Domain Feature-based Expert Diagnostic System for Detection of Hypertension using Photoplethysmogram Signal

Muzaffar Khan^a, Bikesh Kumar Singh^b, Neelamshobha Nirala^c, Mohd. Tahseenul Hasan^d,
Mohammad Nasiruddin^e

Submitted: 10/09/2022 Accepted: 20/12/2022

Abstract: The objective of the present study is to develop an expert diagnostic system for hypertension detection using a photoplethysmogram (PPG) Signal, which overcomes the limitation of the existing model in which accuracy is dependent on quality PPG signals, acquiring high quality can pose a challenge in real-life situations. Our proposed expert diagnostic system uses multi-domain features obtained by combining morphological features and features extracted from the decomposed PPG signal using Variational Mode Decomposition (VMD). ReliefF feature selection is used to select the top 16 features from each feature extraction approach. It is found from the comparative analysis that an expert diagnostic system based on multi-domain features showed significant improvement over the model based on single-domain features. and found to be more immune to noisy PPG signals compared to the single domain-based classification model. A variety of classifiers used are Gradient Boosting Classifier and multilayer perceptron The highest classification accuracy of F1 score for the category normal vs prehypertension, normal vs hypertension type 1 and normal vs hypertension type 2 is found to be 100%, 100% and 100% respectively using hybrid feature and MLP.

Keywords: Hypertension, Photoplethysmogram, Variational Mode Decomposition, Multilayer Perceptron

1. Introduction

Hypertension (HT) is a condition in which Blood pressure values are raised. As per guidelines of the International Society of Hypertension, hypertension is diagnosed when a person's systolic blood pressure (SBP) is ≥ 140 mm Hg and/or diastolic BP (DBP) is ≥ 90 mm Hg. The severity and widespread of hypertension are known from a report published in the year 2017 by the World Health Organization (WHO), in which an estimated 1.13 billion subjects are suffering from hypertension worldwide out of which 10.4 million deaths annually attributed to this raised BP, especially the raised systolic blood pressure (SBP) emerged as a leading risk factor for hypertension [1]. BP is a vital indicator of hypertension and also a leading risk factor for a variety of cardiovascular diseases (CVDs) [2]. Several instruments evolved over the period, for measurement of BP such as the mercury sphygmomanometer is widely regarded as the "gold standard" for blood pressure measurement were phase-out, these device poses an environmental hazard at the time of disposal. The standard location for BP measurement is the brachial artery. Mercury sphygmomanometer is replaced by the auscultatory method which uses an aneroid sphygmomanometer is less accurate and often needs frequent calibration [3]. An automated auscultatory device uses microphones with high sensitivity to detect the Korotokoff sound,

the one with the upper arm cuff is recommended clinically validated. The limitation of cuff based approach lacks a continuous BP monitoring feature. Recent advancements in optical technology, lead to the development of noninvasive optical technology, one such optical technology is known as Photoplethysmography which is successfully used to measure heart rate, oxygen saturation level and rigorously experimented for the development of cuffless measurement of blood pressure (BP) it is still under development process, need to be validated and recommended for clinical use by WHO [2]. The technology which is the dominant and forefront approach which uses the pulse wave analysis (PWA) technique and the machine learning algorithms and is widely reported for the development of cuffless measurement of BP using only one PPG sensor. [4], [5]. The PWA analysis technique is based on identifying fiducial points on the PPG signal which is used for clinical diagnosis, the points are systole peak, dicrotic notch, and dicrotic peak. The PPG signal is formed by summation forwarding propulsion wave during systole cycle of heart and reflected wave during the diastole cycle. The fiducial points are obtained by the first and second derivatives of the main PPG signal. Most of the researchers have proposed a variety of models for hypertension risk stratification using the PWA analysis technique, The PWA approach extract morphological characteristic from the main PPG signal as well as from its first and second derivative such as peak amplitude, time difference, the slope between the various fiducial points on the main PPG signal. The main limitation PWA-based analysis requires a high-quality signal for extracting morphological features based on these points. The limitation of the approach is that the accuracy of the classification model depends on correctly

*muzaffarkhanacet@gmail.com, bsingh.bme@nitrr.ac.in,
neelanir.bme@nitrr.ac.in,
taseenuh@anjumnengg.edu.in, nasiruddin@anjumanengg.edu.in*
Bio-Medical Engineering Department, National Institute of
Technology^{a,b,c} Raipur, Chhattisgarh 492010, India
Artificial Intelligence and Data Science Department, Anjuman
College of Engineering & Technology^{d,e}, India

identifying fiducial points which in turn depend on the quality of the PPG signal [6]. To overcome this limitation, the researcher used a multimodal signal in conjunction with a PPG signal to improve the accuracy, which requires two or more signals such as ECG, and PPT signal which not only increases hardware requirements making it unsuitable for the portable or wearable instrument. Some of the researchers proposed a variety of decomposition techniques such as DWT, and EMD to extract features from decomposed PPG signals and the decomposition technique not only showed improved accuracy but also showed resilience against the noisy PPG signal [7], but lacks the clinical interpretability. The main objective of our study is to develop an expert diagnostic system which overcomes the limitation, the performance of our proposed model is robust to noisy signals and achieves high enough accuracy to be used in clinical diagnosis.

1.2. Related Work

The shortcoming of the Mercury sphygmomanometer and automated auscultatory measurement devices arises from the use of a cuff to be wrapped on the upper arms, then the measurement cycle starts with first recording systole and then Diastole BP values, during which the cuff is inflated and then deflated during the measurement cycle, which makes it unsuitable for continuous BP monitoring. Recently PPG based cuffless blood pressure measurement attracted the attention of researchers due to its simplicity in design and ease of operation. PPG-based diagnostic systems are increasing especially in portable and home monitoring systems such as pulse oximeters, heart rate meters and also to study the property of the arterial tree. The different BP estimation approach used each have some advantages and limitation, the commonly used approaches are Pulse transit time (PTT), Pulse arrival time (PAT) and Pulse wave analysis (PWV) while some researcher used machine learning techniques for BP estimation or hypertension risk assessment. PTT is a technique that uses two PPG sensors, which are placed at two distant sites on the body, two PPG sensors' main function is to measure the distance and time taken by PPG waveforms to travel from the proximal to the distal site, these parameters are used derived diagnostic parameter to study arterial property. There are a few limitations PTT technique, such as frequent calibration required, the use of two sensors increases the complexity, and the precise measurement of the distance between proximal and distal site affects the accuracy of the system, while the PAT technique measures the time interval between the electrical activation of the heart and the arrival of the pulse wave at an arbitrary location on the body such as toe [8]. In case of the PWV technique is based on the theory of wave propagation, which deals with the flow of blood in the blood vessels as a pressure waveform which propagates through central arteries down to smaller distal arteries during systole and diastole cycles respectively [9]. The main limitation of the approach also needs frequent calibration in a short period [10]. In Pulse Wave Analysis approach extracts a morphological feature from the PPG signal and uses a machine-learning algorithm for hypertension detection or estimation of the BP values. Many Researchers used the multi-domain feature-based model to overcome the limitation imposed by the morphological-based diagnostic model in which the accuracy significantly depended on the quality of the PPG signal. In a recently published research paper by Muhammad Umar Khan. [11] in which the proposed model uses multi-domain features which are extracted from the decomposed signal by applying

discrete wavelet transform (DWT) and EMD transform, the features extracted are such as, spectral, time domain, fractal, cepstral, chroma and texture features to achieve overall accuracy of 99.4 % using weighted k-nearest neighbor (KNN-W) classifier. Similarly, J. Leitner et al. [12] proposed a model which uses wavelet decomposition to extract features from the PPG signal and found that the decomposition technique improves the accuracy of the classifier. Wu, Q. [13] proposed a model which uses multi-domain features using wavelet entropy as well as time-domain features and found multi-domain feature-based model improved the classification accuracy. While some researchers not only used multi-domain but also used multiple signals, the other issue encountered by the researcher during classification is a class imbalance, one such study conducted to overcome this problem is conducted by Dipen Deka et al.[14] which demonstrates the advantage of using RUSBoost to overcome class imbalance and achieved an overall F1 score of 0.9347 using multitudinous features extracted from a variety of approaches that are dual-tree complex wavelet packet transform, linear time domain and nonlinear analysis of HRV signal. The limitation of the method is the use of multi-signal not only increases model complexity but also increases computational overheads. Our motivation is to develop an expert diagnostic system that uses multi-domain features and soft computing classification techniques which is robust to noisy signals, using a single PPG.

The contributions of this article are as follows:

1. We developed an expert system for the diagnosis of hypertension using a PPG signal.
2. The proposed expert system uses multi-domain features and a variety of computing techniques to achieve high classification accuracy.

The paper is organized as follows Section 2 explains the material and methods used in this study, while Section 3 describes the feature extraction and feature selection followed by obtained results in Section 4, discussion in Section 5 and conclusion in Section 6.

2. Materials and methods.

Our proposed expert diagnostic system is used for hypertension risk stratification using a PPG signal acquired from the fingertip. The block diagram of the proposed expert diagnostic system is depicted in Figure. 1. The block diagram consists of a signal preprocessing module which performs operations such as PPG filtering and baseline correction, the second block evaluates signal quality index (SQI) and selects the signal based on a predetermined threshold value of SQI. The selected filtered signal is applied to two different modules, the first module extracts morphological features, and the second module decomposes the signal using VMD into a sub-band and extracts features from each sub-band, the statistical features are extracted from the intrinsic mode function (IMF's) of the decomposed signal. ReliefF feature selection algorithm is used to select the top 16 features from each module, the features are applied to the classification module.

2.1. Data Collection

Dataset was acquired from DataCite search which is open clinical trial data for non-invasive detection of cardiovascular disease (CVD), containing 657 data records from 219 subjects in the following category normal (237) prehypertension (258), hypertension Type-I (102), hypertension Type-II (60) The dataset

covers an age range of 20–89 years and records of diseases, including hypertension and diabetes. Data acquisition was carried out under the control of standard experimental [6]. The measurement cycle of 3 minutes duration was used to record three segments of PPG signal of 2.1 seconds duration sampled at 1 kHz,

simultaneously systolic and diastole BP values were measured. The other demographic variable recorded are age, gender, Body Mass Index (BMI), weight and cardiovascular complications.

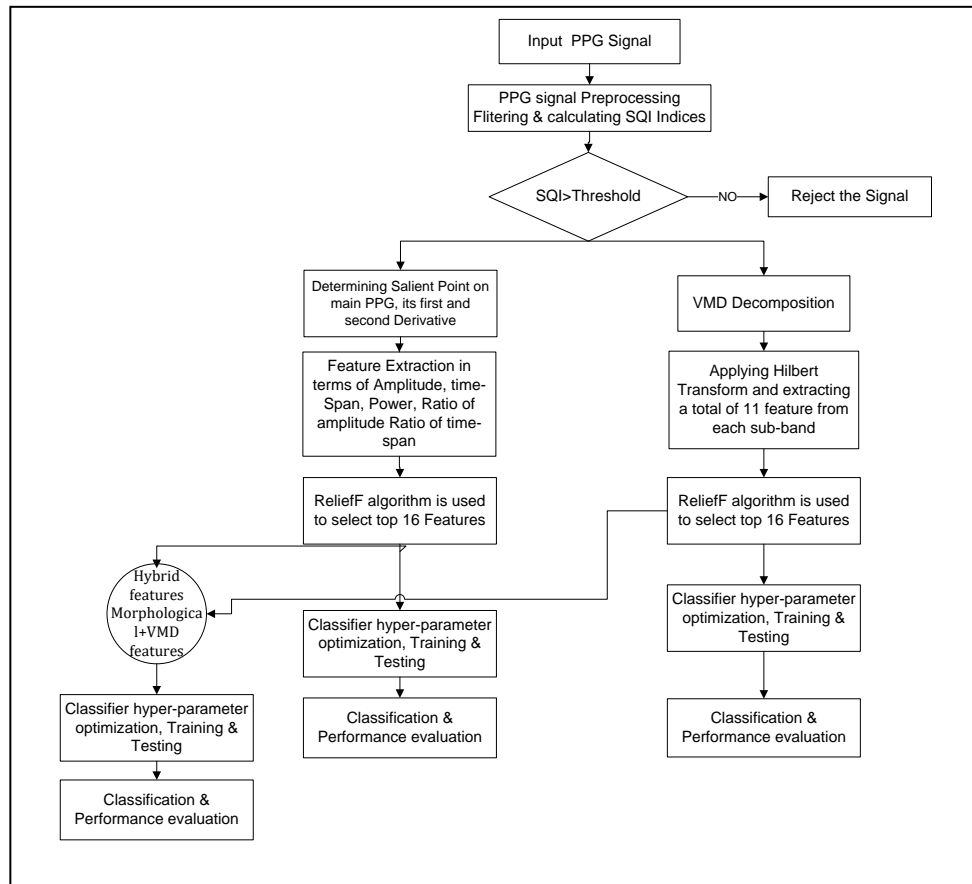


Figure 1: depict a block diagram of the proposed expert diagnostic system for hypertension risk stratification

2.2. Pre-processing

The common sources of noise encountered during PPG signal recording are motion artifacts, respiratory rhythm, and supply source noise. The choice of filter is important to remove noise while retaining vital points on filtered PPG signal such as dicotic peak and dicotic notch, for which to measure the quality of the filtered signal, Signal quality index (SQI) is used, kurtosis (KSQI), entropy (ESQI), we have used three different filters such as Butterworth filter, Elliptic filter and Chebyshev with various filter orders and compared the quality of the signal based SQI obtained from three different filters. The optimal filter is found to be a Chebyshev II, a band-pass filter with the following specification a cut-off frequency of 0.5 and 12 Hz with the 5th order of the filter, validating the finding of Liang, Y. et al.[6].

2.3 Time domain Feature Extraction

A PPG signal carries information not only about changes in blood volume that occurs during the cardiac cycle but also reflects the change in hemodynamics and arterial properties of a cardiovascular system. PPG signal its first derivative (as velocity

Photoplethysmogram (VPG)) and second derivatives (as acceleration Photoplethysmogram (APG)) carry numerous physiological characteristics that have been quantified and used by a large number of researchers in various diagnostic applications such BP estimation, detection hypertension and Diabetes mellitus. Some of the salient points on PPG signal as shown in figure 2, systolic, diastolic peak, dicotic notch, feature extracted are terms of amplitude time-span between the points on main PPG, similarly, features are extracted from the first and second derivative of PPG signal in terms of amplitude and time-span ratio. The feature extraction from the PPG signal and its derivatives was conducted according to the procedure adopted by Elgendi M et al. [15] and Yongbo Liang et al [16]. In total, we have extracted 156 morphological features from PPG, VPG and APG signals in terms of the amplitude of fiducial point, time-span between them, the ratio of amplitude and time-span, slope, waveform area, power between the points which is summarized in table 1

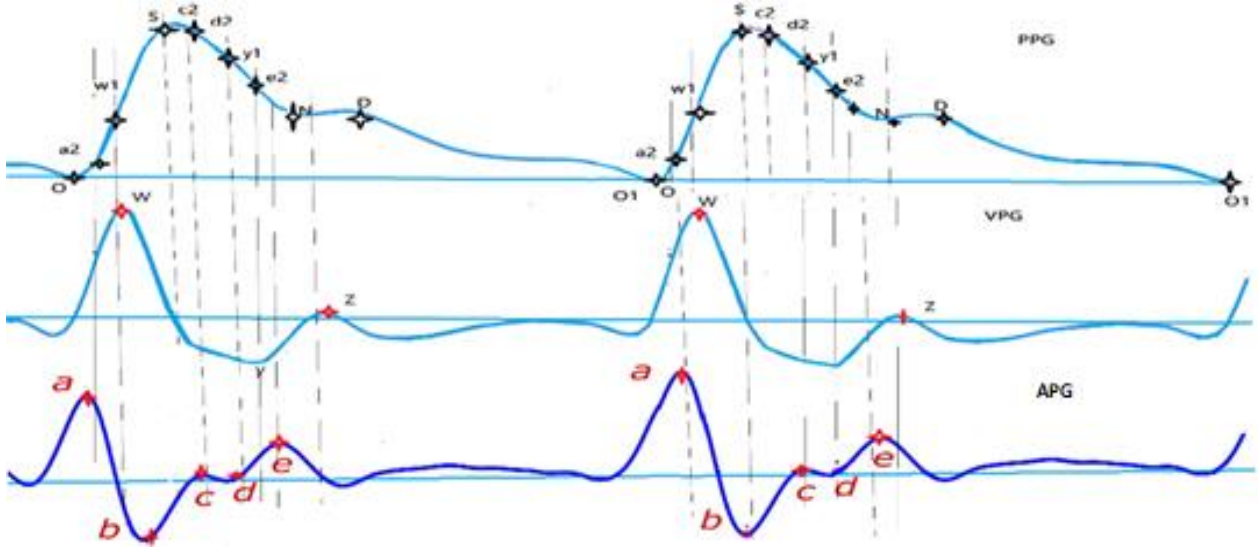


Figure 2. The three signals depicted are the PPG signal, VPG and APG signal respectively.

2.3.2 PPG signal decomposition using Variational mode decomposition technique

Variational mode decomposition (VMD) is a technique which decomposes a signal into different band-limited IMFs. In the proposed model PPG signal is decomposed into a given number of constitutive intrinsic mode functions (IMFs). The bandwidth of IMFs is limited and has a central frequency, the decomposed signal corresponds to a signal like an AM–FM modulated signal. The Hilbert transform is applied to IMF to extract Statistical features from each sub-band. The advantage of the VMD decomposition algorithm is supported by a strong mathematical foundation and the other unique advantage is adaptive in determining optimal bands to estimate corresponding nodes to balance error between them. The VMD algorithm is explained in a summarized way VMD decomposes the signal into its discrete number of modes with specific sparse properties and modes are localized on central frequencies.

1. The signal is transformed into a single-sideband analytic signal using the Hilbert transform.
2. The second operation is termed as complex harmonic mixing, in which the frequency spectrum of each mode to the baseband by mixing with an exponential function tuned to the estimated central frequency.
3. The bandwidth is now estimated through the H1 Gaussian smoothness of the demodulated signal, i.e. the squared bandwidth is estimated using the squared L-2 norm of the gradient subjected to the constraint, detail algorithm and a solution to find the central frequency of each mode is given in the literature [17-19].

3. Feature extraction

In our study, the feature extracted by decomposing PPG signal using VMD transform into a set of narrow-band AM–FM components or IMFs, from which bandwidth is computed for amplitude modulation (BAM) and frequency modulation (BFM) component then Hilbert transform is applied on all IMFs using Welch window 1024 to extract 11 features each IMFs from IMF0 to IMF8 as mention below. Similarly, 11 features of each IMFs from IMF0 to IMF8 are extracted from the sub-band after applying

the VMD transform. The following features extracted from IMFs are as given below.

1. The bandwidth of amplitude modulation component:- where A is the amplitude of the analytic signal, E is the Energy and $\langle \omega \rangle$ is the centre frequency of the current mode, given by Equation [20].

$$BW_{AM}^2 = \frac{1}{E} \int \left(\frac{dA}{dt} \right)^2 \quad (1)$$

2. The bandwidth of the frequency modulation component is given equation 2

$$BW_{FM}^2 = \frac{1}{E} \int \left(\frac{d\phi(t)}{dt} - \langle \omega \rangle \right)^2 A^2(t) dt \quad (2)$$

3. $\langle \omega \rangle$ is the central frequency of the current mode, given by Equation 3.

$$\langle \omega \rangle = \frac{1}{E} \int \frac{d\phi(t)^2}{dt} A^2(t) dt \quad (3)$$

4. Peak Amplitude (Spamp): The peak amplitude of power spectral density (Pxx) for a particular bandwidth is given by

$$Spamp = \max(P_{XX}) \quad (4)$$

5. Peak frequency (Spfreq) is the maximum frequency occurring in normalized Pxx, is given by

$$S_{freq} = \operatorname{argmax}(\overline{P_{XX}}) \quad (5)$$

6. Spectral entropy (SEntropy): is calculated by applying the Shannon entropy concept to the power distribution of the Fourier-transformed signal to measure the uniformity of power spectral density underlying signal. The equation represents spectral entropy

$$S_{entropy} = - \sum_{f=0}^{f_s} \overline{P_{XX}}(f) \log [\overline{P_{XX}}(f)] \quad (6)$$

Where $\overline{P_{XX}}$ denotes normalised spectral density (PSD) of the signal.

7. Spectral centroid (Scent):- The spectral centroid is the centre of mass of the spectrum in which spectrum distribution is defined as the weighted mean of the frequencies presents in the signal, it is used to measure the spectral shape and position of the spectrum of the respective mode,

$$S_{Cent} = \frac{\sum_{f=0}^{f_s} \omega(f) M_{sp}(f)}{\sum_{f=0}^{f_s} M_{sp}(f)} \quad (7)$$

Where f represents frequency bin, $\omega(f)$ (f) and $M_{sp}(f)$ are central frequency and magnitude of the PSD of the bin of f [21].

8. Spectral Energy: -Measures the distribution of signal energy over the frequency band is given as

$$\text{Spectral Energy } (S_{SE}) = \frac{1}{N} \sum_{f=0}^{f_s/2} P_{XX}(f) \quad (8)$$

Where $P_{XX}(f)$ Power Spectral Density is estimated by Welch's Method and N represents a total number of spectral coefficients [22-23].

9. Skewness is related to the measured asymmetry or symmetry distributions of a signal, represented by the following equation:

$$S_{\text{skew}(x)} = E \left[\left(\frac{x(t) - \mu}{\sigma} \right)^3 \right] \quad (9)$$

Where σ represents the standard deviation of signal $x(t)$, and it is mean denoted by μ .

Kurtosis is a measure related to the tail-heaviness of the distribution yielded by the signal and is given by

$$S_{\text{kurt}(x)} = E \left[\left(\frac{x(t) - \mu}{\sigma} \right)^4 \right] \quad (10)$$

10. Hjorth Mobility: The Hjorth parameter comprises a set of three parameters that are Activity, Mobility and Complexity. Hjorth mobility parameter is related to the mean frequency of the signal and proportional to variance in the spectrum and expressed as a ratio per time unit. The Hjorth mobility is represented by the equation as given below [24-25]

$$Hj_{\text{Mob}}(x) = \sqrt{\frac{\text{var}(dx(t)/dt)}{\text{var}(x(t))}} \quad (11)$$

11. Hjorth Complexity: a measure of the standard deviation of the slope with reference to the standard deviation of the amplitude

$$Hj_{\text{com;p}}(x) = \sqrt{\frac{Hj_{\text{mob}}(dx(t)/dt)}{Hj_{\text{mob}}(x(t))}} \quad (12)$$

The features extracted from IMFs are Differential entropy, Peak-magnitude of root-mean-square ratio (PRMS) [26]. then these IMF obtained are subjected to Hilbert transform to yield AM and FM frequencies then the second category of the features extracted are as follows (i) spectral peak magnitude, peak frequency, (ii) spectral entropy (iii) spectral energy [27]. The detail of 156 morphological features is shown in table 1 and table 2 depicts a total of 16 features selected extracted out of 99 features extracted from IMF 0 to IMF8. Similarly, A total of 16 features are selected out of 156 morphological features extracted.

3.1. Feature selection and classifier Optimization:

The general feature selection technique is categorized into a filter, wrapper and embedded, each offering unique advantages and limitations. The filter method uses ranking based on a statistical approach which is fast and functions are independent of the induction algorithm, while the wrapper employs any stand-alone modelling algorithm to train a predictive model using a candidate feature subset [28]. We chose the ReliefF feature selection algorithm because it is computationally efficient

and sensitive to complex patterns of an association through correctly estimating the quality of attributes in classification problems with strong dependencies between attributes, by exploiting local information. ReliefF algorithm is summarised as the search algorithm randomly selecting an instance, then updates quality estimation parameter vector W for all attributes the with and without dependencies among them, based on searches for k nearest neighbours from the same class, called nearest hits and that from the different classes, called the nearest misses. The value of k is set to an arbitrary small number, default value k is set to 10 [29]. ReliefF algorithm overcomes the limitation of relief that is it can deal with more than two class problems and works well with incomplete data or noisy data. The relief algorithm can be found in the literature [30].

Hyperparameters are important for machine learning algorithms since they directly control the behaviours of training algorithms and have a significant effect on the performance of machine learning models. Several techniques have been developed

Table 2: depicts the time domain and VMD feature selected using the ReliefF algorithm

s.no	Time Domain	VMD
1	$\overline{SN}/\overline{OO_1}$	pow2
2	$\overline{b_2 o}/\overline{OO_1}$	pk7
3	d_amp/a_amp	pow4
4	$\overline{Sd_2}/\overline{O_1 S}$	pow7
5	$\overline{a_2 w_1}/\overline{OO_1}$	Cent0
6	$\overline{Sc_2}/\overline{OO_1}$	AM8
7	$\overline{c_2 o_1}$	Cent7
8	\overline{SN}	pk2
9	$\overline{Se_2}/\overline{OO_1}$	kurt3
10	$\overline{So}/\overline{O_1 S}$	Hcomp6
11	$\overline{Sc_2}$	pow3
12	$\overline{os}/\overline{OO_1}$	kurt0
13	$\overline{d_2 o}/\overline{OO_1}$	BM7
14	$\overline{SN}/\overline{N O_1}$	skew1
15	b_amp/a_amp	freq1
16	$\overline{b_2 N}/\overline{OO_1}$	pk3

and successfully applied for certain application domains. A Grid Search Optimization (GSO) technique is used to optimize the classifier since GSO is computationally efficient when training the classifier over a large data set [31].

3.2 Classification and performance evaluation

The proposed expert diagnostic system uses classifiers such as Gradient Boosting Classifier (GB), Multi-Layer Perceptron (MLP) and Sequential deep Learning neural network for the classification of normal versus different severity of hypertension.

Table 1:- A total of 156 morphological features are extracted from the PPG signal, the first and its second derivative is listed below.

Amplitude of point First derivative (3), Amplitude of point second from derivative amplitude (5) & ratio of amplitude point (11)			
1. \overline{oS} , 2. $\overline{Sc_2}$, 3. $\overline{ob_2}$, 4. $\overline{a_2 o}$, 5. \overline{SN} -late systole, 6. \overline{SD} -Early diastolic duration, 7. $\overline{SY_1}$, 8. $\overline{Se_2}$, 9. $\overline{No_1}$ -- Diastole duration, 10. $\overline{oo_1}$ -Pulse duration, 11. $\overline{a_2 w_1}$, 12. $\overline{b_2 w_1}$, 13. $\overline{w_1 y_1}$, 14. $\overline{b_2 o_1}$, 15. $\overline{c_2 o_1}$, 16. $\overline{d_2 o_1}$, 17. $\overline{a_2 b_2}$, 18. $\overline{Sb_2}$, 19. $\overline{d_2 c_2}$, 20. $\overline{Y_1 d_2}$, 21. $\overline{e_2 y_1}$, 22. $\overline{b_2 N}$, 23. $\overline{Y_1 o_1}$, 24. $\overline{e_2 o_1}$, 25. \overline{Nd} , 26. $\overline{o_1 S}$, 27. $\overline{w_1 o_1}$, 28. $\overline{Sw_1}$, 29. $\overline{o_1 d}$, 30. $\overline{w_1 S}$			
Slope between the point on PPG (16)			
1. slopeoS 2. slopeow ₁ 3. slopeSN 4. slopeNO ₁ 5. slopew ₁ b ₂ 6. slopeND 7. slopeo ₁ 8. slopeNo ₂ 9 slopeow ₁ 10. slopeb ₂ S 11. slopee ₂ y ₁ . 12. slopey ₁ d ₂ 13. slopee ₂ y ₁ 14. slopeNe ₂ 15. slopeo ₁ S. 16. slopeoa ₂ .			
Area ratio of PPG signal (6)			
1. Areatatio1 = $(\overline{Sb}/\overline{oo_1})$. 2. Areatatio2 = $(\overline{oa_2}/\overline{oo_1})$. 3. Areatatio3 = $(\overline{oN}/\overline{oo_1})$. 4. Areatatio4 = $(\overline{SN}/\overline{oo_1})$. 5. Areatatio5 = $(\overline{oD}/\overline{oo_1})$. 6. Areatatio6 = $(\overline{Doo_1}/\overline{oo_1})$			
Time-span Ratio of different points on PPG signal (42)			
1. tspanratio = $\overline{os}/\overline{oo_1}$	2. tspanratio = $\overline{ao}/\overline{oo_1}$	3. tspanratio = $\overline{a_2 b_2}/\overline{oo_1}$	4. tspanratio4 = $\overline{ob_2}/\overline{oo_1}$
5. tspanratio = $\overline{SN}/\overline{oo_1}$	6. tspanratio6 = $\overline{SD}/\overline{oo_1}$	7. tspanratio7 = $\overline{Sc_2}/\overline{oo_1}$	8. tspanratio8 = $\overline{Sd_2}/\overline{oo_1}$
9. tspanratio9 = $\overline{SY_1}/\overline{oo_1}$	10. tspanratio10 = $\overline{NO}/\overline{oo_1}$	11. tspanratio11 = $\overline{a_2 w_1}/\overline{oo_1}$	12. tspanratio12 = $\overline{o_1 D}/\overline{oo_1}$
13. tspanratio13 = $\overline{Se_2}/\overline{oo_1}$	14. tspanratio14 = $\overline{b_2 w_1}/\overline{oo_1}$	15. tspanratio15 = $\overline{Sb_2}/\overline{oo_1}$	16. tspanratio16 = $\overline{d_2 c_2}/\overline{oo_1}$
17. tspanratio17 = $\overline{y_1 d_2}/\overline{oo_1}$	18. tspanratio18 = $\overline{w_1 y_1}/\overline{oo_1}$	19. tspanratio19 = $\overline{b_2 N}/\overline{oo_1}$	20. tspanratio20 = $\overline{w_1 y_1}/\overline{oo_1}$
21. tspanratio21 = $\overline{b_2 o}/\overline{oo_1}$	22. tspanratio22 = $\overline{c_2 o}/\overline{oo_1}$	23. tspanratio23 = $\overline{d_2 o}/\overline{oo_1}$	24. tspanratio24 = $\overline{y_1 o_1}/\overline{oo_1}$
25. tspanratio25 = $\overline{e_2 o_1}/\overline{oo_1}$	26. tspanratio26 = $\overline{ao}/\overline{os}$	27. tspanratio27 = $\overline{b_2 o_2}/\overline{oo_1}$	28. tspanratio28 = $\overline{os}/\overline{o_1 s}$
29. tspanratio29 = $\overline{SN}/\overline{No_1}$	30. tspanratio30 = $\overline{Sc_2}/\overline{o_1 S}$	31. tspanratio31 = $\overline{Sd_2}/\overline{o_1 S}$	29. tspanratio32 = $\overline{SY_1}/\overline{o_1 S}$
33. tspanratio33 = $\overline{Se_2}/\overline{o_1 S}$	34. tspanratio34 = $\overline{So}/\overline{o_1 S}$	35. tspanratio35 = $\overline{d_2 c_2}/\overline{y_1 d_2}$	36. tspanratio36 = $\overline{y_1 d_2}/\overline{o_1 S}$
37. tspanratio37 = $\overline{e_2 y_1}/\overline{d_2 c_2}$	38. tspanratio38 = $\overline{e_2 y_1}/\overline{y_1 d_2}$	39. tspanratio39 = $\overline{Dc_2}/\overline{y_1 d_2}$	40. tspanratio40 = $\overline{ND}/\overline{No_1}$
41. tspanratio41 = $\overline{Sw_1}/\overline{Sy_1}$	42. tspanratio42 = $\overline{Sa_2}/\overline{Sy_1}$		
Amplitude of point First derivative (3), Amplitude of point second from derivative amplitude (5) & ratio of amplitude point (11)			
1. <i>W_amp</i> – VPG positive amplitude 2. <i>y_amp</i> – VPG negative amplitude 3. <i>z_amp</i> - VPG second positive amplitude			
1. <i>a_amp</i> -Early systolic positive wave 2. <i>b_amp</i> – Early systolic negative wave. 3. <i>c_amp</i> —Late systolic wave			
4. <i>d_amp</i> -Late systolic decreasing wave 5. <i>e_amp</i> -Early diastole 6. <i>ratioa</i> = <i>b_amp</i> / <i>a_amp</i>			
7. <i>ratioa</i> = <i>c_amp</i> / <i>a_amp</i> arterial. stiffness 8. <i>ratioa</i> = <i>d_amp</i> / <i>a_amp</i> 9. <i>ratioa</i> = <i>e_amp</i> / <i>a_amp</i>			
10. <i>ratiobcdebya</i> = (<i>b_amp</i> - <i>c_amp</i> - <i>d_amp</i> - <i>e_amp</i>) / <i>a_amp</i> -AGI 11. <i>ratiobcdebya</i> = (<i>b_amp</i> - <i>c_amp</i> - <i>d_amp</i>) / <i>a_amp</i> -aging index(AI)			
Point derived on main PPG from the first and second derivative (16)			
1. <i>a_2_amp</i> . 2. <i>b_2_amp</i> 3. <i>c_2_amp</i> 4. <i>o_1_amp</i> 5. <i>w_2_amp</i> 6. <i>d_2_amp</i> 7. <i>e_2_amp</i> 8. <i>y_1_amp</i> 9. <i>D_amp</i> -Dicrotic peak 10. <i>N_amp</i> -Notch 11. <i>S_amp</i> - peak systole amplitude. 12. <i>o_amp</i> -minimum diastole value. 13. <i>ratiow_1s</i> = <i>w_1_amp</i> / <i>S_amp</i> 14. <i>ratiob_2s</i> = <i>b_2_amp</i> / <i>S_amp</i> 15. <i>ratioNS</i> = <i>N_amp</i> / <i>S_amp</i> -augmentation index. 16. <i>ratioc_2s</i> = <i>c_2_amp</i> / <i>S_amp</i> .			
Power Calculated from different segments of PPG signal (19)			
1. $\overline{ospower}$. 2. $\overline{oo_1 totalpower}$. -Pulse power. 3. $\overline{NDpower}$. 4. $\overline{oa_2 power}$. 5. $\overline{sd_2 power}$ 6. $\overline{sy_1 power}$ 7. $\overline{se_2 power}$ 8. $\overline{SNpower}$. 9. $\overline{SDpower}$. 10. $\overline{So_1 power}$. 11. $\overline{a_2 w_1 power}$. 12. $\overline{b_2 Spower}$. 13. $\overline{Ne_2 power}$. 14. $\overline{Ne_1 power}$ 15. $\overline{w_1 b_2 power}$. 16. $\overline{y_1 d_2 power}$. 17. $\overline{e_2 y_1 power}$ 18. $\overline{o_1 Dpower}$. 19. $\overline{Sc_2 power}$			

The main reason for choosing GB classifier it provides high accuracy and low bias. The GB classifier algorithm is based on combining weak learners, Decision trees are used as the weak learner in GB, the decision tree is constructed using a greedy algorithm, and the best split points are based on purity scores like Gini or to minimize the loss. A gradient descent procedure is used to minimize the loss when adding trees. Some of the important parameters are the number of trees added, the second constraint is the depth of the tree greater depth increases complexity, sub-sampling is about selecting the sample of data for training while the learning rate controls the number of trees added to minimize the loss function. The detailed algorithm can be found in the literature [32].

The multilayer perceptron (MLP) generalized structure consists of an input layer, hidden layer and output layer that are interconnected neurons, also known as nodes, MLP maps between an input vector with the output vector using connection with weights assigned to each connection and the output signals which are a function of the sum of the inputs to the node multiplied by weights and modified by activation, function at the output layer, the weights are adjusted

using an iterative process to establish a relation between input and output using back-propagation algorithm [33-34].

The Keras package is used to implement the structure of various layers of sequential neural networks with their associated parameters and corresponding activation functions are depicted in figure 2. It consists of a dense layer which consists of neuron nodes and an activation function which maps functions having negative values to zero or a positive value by a function known as a Rectified linear unit (ReLU). The pooling layer performs nonlinear downsampling, reducing the number of parameters that the network needs to learn [35-36].

The classifiers are trained and tested using 10-fold cross-validation for performance evaluation and comparison of hypertension risk stratification and DM-II detection models using parameters such as accuracy (ACC), sensitivity (SE), positive predictive (PP), and F1-score (F1). The most important step before the training and testing phase is to identify and remove outliers that can significantly deteriorate the classifier's performance.

Table 3: depicts Classification results Obtained for categories Normal versus Prehypertension, Normal versus hypertension type I and Normal versus hypertension type II for Morphological and multidomain features.

Normal Vs Prehypertension		(Feature type:- Morphological features & features selection algorithm)								
Normal sample size =240 pre hypertension sample size = 254 CV=10 fold		(Classification strategy :one vs one)Number of features :16								
Classifier/Kernal Parameters/ optimization technique	TP	FN	FP	TN	SE%	SP%	ACC %	AUC	Precision	F1%
Gradient Boosting {'learning_rate': 0.01, 'max_depth': 3, 'n_estimators': 50, 'subsample': 0.7}	170	70	58	200	70.8	77.5	74.1	1.00	0.75	74
MLP (150,100,50), ax_iter=300,activation 'relu',solver='adam'	237	3	0	258	98.7	100	99.3	0.97	0.99	99
Sequential deep Learning Neural Network	226	14	4	254	94.2	98.4	96	0.73	0.73	76
Normal Vs Prehypertension		(Feature type: :- Morphological features (16)+ VMD features (16))								
Gradient Boosting Classifier {'learning_rate': 0.01, 'max_depth': 100, 'n_estimators': 50, 'subsample': 0.7}	191	49	45	213	79.6	82.6	81	0.81	0.81	81.9
MLP (150,100,50), max_iter=300,activation 'relu',solver='adam'	240	0	0	258	100	100	100	1	1	100
Sequential deep Learning Neural Network	184	56	3	255	76.7	98.8	88.1	0.87	0.90	87
Normal Vs hypertension type 1		(Feature type: - Morphological features & features selection algorithm)								
Normal sample size =240 pre hypertension sample size = 105 CV=10 fold		(Classification strategy :one vs one)Number of features :16								
Gradient Boosting Classifier {'learning_rate': 0.01, 'max_depth': 3, 'n_estimators': 100, 'subsample': 0.5}	237	3	62	43	98.8	41.0	0.81	0.7	0.81	57
MLP (150,100,50), max_iter=300,activation 'relu',solver='adam'	239	1	0	105	99.6	100	99	0.99	0.99	98.8
Sequential deep Learning Neural Network	229	11	8	97	95.4	92.4	95.6	0.93	0.96	.93
Normal Vs hypertension type 1		(Feature type: :- Morphological features (16)+ VMD features (16))								
Gradient Boosting Classifier ,'_rate': 0.01, 'max_depth': 3,'n_estimators': 50, 'subsample': 0.5}	240	0	1	104	100.	99.0	100	0.99	0.99	100
MLP (150,100,50), max_iter=300,activation 'relu',solver='adam'	240	0	0	105	100.	100.	100	1	1	100
Sequential deep Learning Neural Network	234	6	0	105	97.5	100	0.98	0.98	0.97.	97.5
Normal Vs hypertension type 2		(Feature type:- Morphological features & features selection algorithm)								
Normal sample size =240 hypertension type 2 sample size = 54 CV=10 fold		(Classification strategy :one vs one)Number of features :16								
Gradient Boosting {'learning_rate': 0.01, 'max_depth': 3, 'n_estimators': 50, 'subsample': 0.5}	240	0	11	43	100.	79.6	85	0.99	0.81	100
MLP (150,100,50), max_iter=300,activation 'relu',solver='adam'	235	5	17	37	97.9	68.5	93	0.85	0.93	97.9
Sequential deep Learning Neural Network	236	4	18	36	98.3	66.7	91.8	0.80	0.90	98.3
Normal Vs hypertension type 2		(Feature type: :- Morphological features (16)+ VMD features (16))								
Gradient Boosting Classifier'_rate': 0.01, depth': 3, 'n_estimators': 50, 'subsample': 0.5}	240	0	1	53	100.	98.1	100	0.99	0.99	100
MLP (150,100,50), max_iter=300, activation 'relu',solver='adam'	240	0	0	54	100	100	100	1	1	100
Sequential deep Learning Neural Network	240	0	0	54	100	100	100	1	1	100

We have considered a low outlier, whose value is less than $Q1-1.5$ (IQR) while the upper outlier has values greater than $Q1+1.5$ (IQR) where IQR denotes an interquartile range. We have considered a low outlier, whose value is less than $Q1-1.5$ (IQR) while the upper outlier has values greater than $Q1+1.5$ (IQR) where IQR denotes an interquartile range. We had opted for a one versus one classification strategy to overcome the class imbalance problem that generally occurs in one Vs all classification strategy. The error rate is a commonly used parameter for

for comparing the performance of the classifier, but we have used the F1 score since there was a class imbalance problem and also provide the result in terms of a false positive and false negative for comparison purposes. The K-fold cross-validation over the holdout method of validation to avoid overfitting and underfitting problems. The classifiers were tuned using Grid optimization which offers faster tuning and avoids overfitting. While Adam's optimization technique is used for tuning neural network parameters which provides faster convergence [37-38].

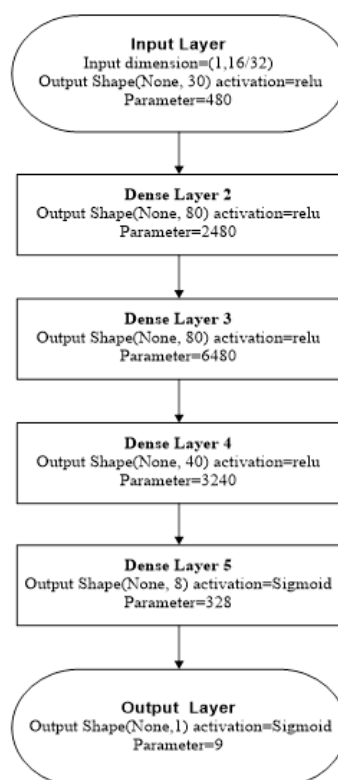


Figure 2 depicts the structure of a sequential deep learning neural network

4. Results

From the result obtained as shown in Table 3, It is found that multilayer perceptron which uses hybrid feature achieved the overall high classification among the classifier which uses VMD feature or morphological-based features. the F1 score achieved for the category normal vs prehypertension, normal vs hypertension type 1 and normal vs hypertension type 2 are 100%, 100% and 100% respectively. The main difficulty poses by the multilayer perceptron classifier while setting an optimal number of neurons in input, hidden layer and number of iterations to avoid overfitting and underfitting issue. The Gradient boosting classifier with the use of multi-domain features has shown a low F1 score of 57% for category normal vs prehypertension. During optimization of gradient boosting classifier parameter using grid optimization technique large number of the estimator and subsample are required. In the case of Sequential deep learning that uses multidomain features has shown a low F1 score as compared to multilayer perceptron for the category normal vs prehypertension and designing the structure and setting internal parameters is a meticulous task and demand high computational resources.

5. Discussion

From the comparison between the result obtained among the classifier that uses a single domain feature with the classifier that uses a hybrid, it is found that using multi-domain features classifiers have shown significant improvement in the classification accuracy. It is observed that the top 16 morphological features mostly contain the ratio of time-span feature and the time duration from systolic peak to diastole notch which is in line with the previous finding reported by Liang, Y et al [39]. The second observation complies with the first observation we find a ratio time-span of the second derivative PPG signal which overlaps late systolic cycle time duration. While in the case of features selected using VMD, the power and central frequency feature appears at top of the selected feature list as depicted in table 2. The multi-domain contains a total of 32 features obtained by combining 16 features of VMD-based feature extraction with a total of 16 morphological features. Grid search is used to tune GB classifier, MLP uses backpropagation algorithm and sequential neural network using Adam optimization technique, the optimizer uses stochastic gradient descent method that is based on adaptive estimation of first-order

and second-order moments. The advantage of Adam optimization is computational and memory efficient and well suited for large data classification.

6. Conclusion

It is concluded from the result obtained that the multi domain-based feature improves the accuracy of the classification model as compared to a single domain that is morphological. Ours proposed a framework that uses a hybrid feature-based expert diagnosis system which makes the system more immune to noisy signals and overcomes the limitation of an expert diagnostic model that requires a high-quality PPG signal to extract morphological features. The main advantage of our proposed model is that it not only retains clinical interpretability for cross-examination of the result and maintains performance classification accuracy when subjected to the noisy PPG signal. Our proposed model exploits the quality of the VMD technique to transform the signal into narrowband intrinsic function resulting increase in noise immunity. We plan to extend our work in future to improve the proposed methodology in terms of using an advanced technique which is fast in computation and require optimal resources to be deployed on mobile and web application. The limitation of our study is the use of a smaller dataset and the need to quantify the noise immunity of the model and plan to use the meta-heuristics optimization technique which overcomes the limitation grid search algorithm that it works efficiently only when a number of the feature are small [40].

Declarations section

Acknowledgements: We are thankful to the DRC committee member for their unwavering support and motivation to carry out research work. We also thank the Director of NIT Raipur to provide all the help and resource, providing a conducive environment to carry out the research work.

Author contributions:

Data Citation: Liang, Y., Liu, G., Chen, Z. & Elgendi, M. figshare. <https://doi.org/10.6084/m9.figshare.5459299.v2> (2017).

Authors' contributions: Authors equally contributed to writing, reading, and approving the final

Conflicts of interest: The authors declare no conflicts of interest.

References

[1] Jeffrey D Stanaway et al, "Global, regional, and national comparative risk assessment of 84 behavioural, environmental and occupational, and metabolic risks or clusters of risks for 195 countries and territories", 1990–2017: a systematic analysis for the Global Burden of Disease Study 2017, (2018).

[2] Oommen John et al., "WHO technical specifications for automated non-invasive blood pressure measuring devices with cuff. Geneva: World Health Organization"; (2020) ISBN 978-92-4-000266-1.

[3] Siddique, Sarkar and Chow, James C. L., "Machine Learning in Healthcare Communication", Journal Encyclopedia, VOL1, PP 220–239 <https://www.mdpi.com/2673-8392/1/1/21>, ISSN 2673-8392, (2021).

[4] Garg, D. K. . (2022). Understanding the Purpose of Object Detection, Models to Detect Objects, Application Use and Benefits. International Journal on Future Revolution in Computer Science & Communication Engineering, 8(2), 01–04. <https://doi.org/10.17762/ijfresce.v8i2.2066>

[5] Y. Kurylyak, F. Lamonaca and D. Grimaldi, "A Neural Network-based method for continuous blood pressure estimation from a PPG signal," *2013 IEEE International Instrumentation and Measurement Technology Conference (I2MTC)*, 2013, pp. 280-283, DOI: 10.1109/I2MTC.2013.6555424.

[6] C. El-Hajj and P.A. Kyriacou, "A review of machine learning techniques in photoplethysmography for the non-invasive cuffless measurement of blood pressure", *Biomedical Signal Processing and Control* Vol no 58, PP 101870,2020,ISSN :1746-8094 DOI :<https://doi.org/10.1016/j.bspc.2020.101870>.

[7] Liang, Y, Elgendi, M., Chen, Z. et al., "An optimal filter for short photoplethysmogram signals", *Sci Data* 5, 180076, (2018), <https://doi.org/10.1038/sdata.2018.76>

[8] Jaypal Singh Rajput et al. (2021), "Automated detection of hypertension using wavelet transform and nonlinear techniques with ballistocardiogram signals", *Informatics in Medicine Unlocked*, Volume 26, 2021, 100736, ISSN 2352-9148, <https://doi.org/10.1016/j.imu.2021.100736>.

[9] R. Mukkamala et al., "Toward Ubiquitous Blood Pressure Monitoring via Pulse Transit Time: Theory and Practice," in *IEEE Transactions on Biomedical Engineering*, vol. 62, no. 8, pp. 1879-1901, Aug. (2015), DOI: 10.1109/TBME.2015.2441951.

[10] Wagenseil, J.E., Mecham, R.P., "Elastin in Large Artery Stiffness and Hypertension", *J. of Cardiovasc. Trans. Res.* 5, 264–273 (2012). <https://doi.org/10.1007/s12265-012-9349-8>.

[11] A. Esmaili, M. Kachuee and M. Shabany, "Nonlinear Cuffless Blood Pressure Estimation of Healthy Subjects Using Pulse Transit Time and Arrival Time", *IEEE Transactions on Instrumentation and Measurement*, vol. 66, no. 12, pp. 3299-3308, Dec. (2017), DOI: 10.1109/TIM.2017.2745081.

[12] Muhammad Umar Khan et al., "Expert Hypertension Detection System Featuring Pulse Plethysmograph Signals and Hybrid Feature Selection and Reduction Scheme", *Sensors*, vol no 21, PubMedID: 33401652, ISSN 1424-8220, (2021), DOI:10.3390/s21010247.

[13] J. Leitner, P. -H. Chiang and S. Dey, "Personalized Blood Pressure Estimation Using Photoplethysmography: A Transfer Learning Approach," in *IEEE Journal of Biomedical and Health Informatics*, vol. 26, no. 1, pp. 218-228, Jan. 2022, DOI: 10.1109/JBHI.2021.3085526.

[14] Wu, Q, "On a Feature Extraction and Classification Study for PPG Signal Analysis", *Journal of Computer and Communications*, 9, 153-160, (2021), <https://doi.org/10.4236/jcc.2021.99012>.

[15] Dipen. Deka, B. Deka, "Stratification of HRH Patients Using Hybrid HRV Features and Boosting Algorithms", DOI 10.1109/ACCESS.2021.3074967, (2021), IEEE Access.

[16] Elgendi M, Liang Y, Ward R, "Toward Generating More Diagnostic Features from Photoplethysmogram Waveforms", *Diseases*. (2018); 6(1):20. <https://doi.org/10.3390/diseases6010020>

[17] Liang, Y., Chen, Z., Ward, R., & Elgendi, M., "Hypertension Assessment Using Photoplethysmography: A Risk Stratification Approach", *Journal of clinical medicine*, 8(1), 12, (2018). <https://doi.org/10.3390/jcm8010012>

[18] C. Montalvo, C.J. Gavián, A. García-Berrocal, "Variational mode decomposition method (VMD) applied to Decay Ratio (DR) calculation for instabilities identification in BWR" *Nuclear Engineering and Design*, Volume 390,2022, ISSN 0029-5493, <https://doi.org/10.1016/j.nucengdes.2022.111702>.

[19] Salimi S, Koochaki A., "An Effective Method for Islanding Detection Based on Variational Mode Decomposition", *Electrica*, 2019; 19(2): 135-1145, (2014).

- [20] R. Satheesh et al, "Identification of Oscillatory Modes in Power System Using Deep Learning Approach", *IEEE Access*, open access Journal, DOI:10.1109/ACCESS.2022.3149472, (2022), [cross reference].
- [21] Cohen L et al., "Instantaneous bandwidth for signals and spectrogram", *Int Conf Acoust Speech, Signal Process. IEEE*; 2451–2454, (1990). DOI:10.1109/ICASSP.1990.116086.
- [22] C. J. Huang, Y. J. Yang, D. X. Yang, and Y. J. Chen. "Frog classification using machine learning techniques". *Exp Sys with App*.36: 3737–3743. (2009).
- [23] Welch P, "The use of fast Fourier transform for the estimation of power spectra: A method based on time averaging over short, modified periodograms", *IEEE Trans Audio Electroacoustic*. 15: 70–73. (1967), DOI:10.1109/TAU.1967.1161901.
- [24] Malla, S., M. J. Meena, O. Reddy, R. V. Mahalakshmi, and A. Balobaid. "A Study on Fish Classification Techniques Using Convolutional Neural Networks on Highly Challenged Underwater Images". *International Journal on Recent and Innovation Trends in Computing and Communication*, vol. 10, no. 4, Apr. 2022, pp. 01-09, doi:10.17762/ijritcc.v10i4.5524.
- [25] Gilles, Jérôme, "Empirical Wavelet Transform", *IEEE Transactions on Signal Processing* 61, no. 16: 3999–4010, (2013), <https://doi.org/10.1109/TSP.2013.2265222>.
- [26] Vourkas, M. & Sifis, Micheloyannis & Papadourakis, Giorgos, "Use of ANN and Hjorth parameters in mental-task discrimination. Advances in medical signal and information processing", 2000 First international conference on (IEE conf publ no 476). (2000) 327 - 332. 10.1049/cp:20000356
- [27] Navascués MA, Sebastián M V, "Time-domain indices and discrete power spectrum in electroencephalographic processing", *Int J Comput Math*;86 1968–1978, (2009) DOI:10.1080/00207160903023599.
- [28] Ravi Kumar, M., Srinivasa Rao, Y, "Epileptic seizures classification in EEG signal based on semantic features and variational mode decomposition.Cluster", *Comput* 22, 13521–13531, (2019). <https://doi.org/10.1007/s10586-018-1995-4>.
- [29] Martis RJ, Acharya UR, Tan JH, Petznick A, Yanti R, Chua CK, Ng EY, Tong L., "Application of empirical mode decomposition for automated detection of epilepsy using EEG signals", *Int J Neural Syst.*, (2012) Dec;22(6):1250027. (2012), DOI: 10.1142/S012906571250027X
- [30] Ryan J. Urbanowicz, et al, "Relief-based feature selection: Introduction and review", *Journal of Biomedical Informatics*, Volume 85, Pages 189–203, ISSN:1532-0464, (2018), <https://doi.org/10.1016/j.jbi.2018.07.014>.
- [31] Abdullah Y. Muaad et al, "Arabic Document Classification: Performance Investigation of Preprocessing and Representation Techniques", *Mathematical Problems in Engineering*, Article ID 3720358, 16 pages, (2022). <https://doi.org/10.1155/2022/3720358>.
- [32] Alotaibi, A.S, "Hybrid Model Based on ReliefF Algorithm and K-Nearest Neighbor for Erythematous-Squamous Diseases Forecasting", *Arab J Sci Eng* 47, 1299–1307, (2022) <https://doi.org/10.1007/s13369-021-05921-z>
- [33] G. Behera and N. Nain, "Grid Search Optimization (GSO) Based Future Sales Prediction for Big Mart," 15th International Conference on Signal-Image Technology & Internet-Based Systems (SITIS), pp. 172-178, (2019), DOI: 10.1109/SITIS.2019.00038.
- [34] Bentéjac, Candice, "A comparative analysis of gradient boosting algorithms, *Artificial Intelligence Review*", (2021) DOI: 10.1007/s10462-020-09896-5.
- [35] J. Mateo et al, "Extreme gradient boosting machine learning method for predicting medical treatment in patients with acute bronchiolitis", *Biocybernetics and Biomedical Engineering*, Volume 41, Issue 2, Pages 792-801, ISSN 0208-5216, (2021), <https://doi.org/10.1016/j.bbe.2021.04.015>
- [36] Guanwei Yin, Fouad Jameel Ibrahim et al., "Machine learning method for simulation of adsorption separation: Comparisons of model's performance in predicting equilibrium concentrations", *Arabian Journal of Chemistry*, Volume 15, Issue 3103612, ISSN 1878-5352, (2022), <https://doi.org/10.1016/j.arabjc.2021.103612>.
- [37] Maxime Voisin et al, "Ambulatory Atrial Fibrillation Monitoring Using Wearable Photoplethysmography with Deep Learning", *Medical Physics (physics.med-ph)*, (2018) <https://doi.org/10.48550/arXiv.1811.07774>.
- [38] Gulli, Antonio, and Sujit Pal. *Deep learning with Keras*. Packt Publishing Ltd, (2017).
- [39] J. Nowak, et al. "Discovering Sequential Patterns by Neural Networks," 2020 International Joint Conference on Neural Networks (IJCNN), pp. 1-6, DOI: 10.1109/IJCNN48605.2020.9207461.
- [40] Yan Huang, et al, "A modified scale-space guiding variational mode decomposition for high-speed railway bearing fault diagnosis", *Journal of Sound and Vibration*, Volume 444, Pages 216-234, ISSN 0022-460X, <https://doi.org/10.1016/j.jsv.2018.12.033>, (2019).
- [41] Sudhakar, C. V., & Reddy, G. U. (2022). Land use Land cover change Assessment at Cement Industrial area using Landsat data-hybrid classification in part of YSR Kadapa District, Andhra Pradesh, India. *International Journal of Intelligent Systems and Applications in Engineering*, 10(1), 75–86. <https://doi.org/10.18201/ijisae.2022.270>.
- [42] Liang, Y., Chen, Z., Ward, R., & Elgendi, M, "Hypertension Assessment Using Photoplethysmography: A Risk Stratification Approach", *Journal of clinical medicine*, 8(1), 12. (2018). <https://doi.org/10.3390/jcm8010012>
- [43] André Sanches Fonseca Sobrinho. (2020). An Embedded Systems Remote Course. *Journal of Online Engineering Education*, 11(2), 01–07. Retrieved from <http://onlineengineeringeducation.com/index.php/joe/article/view/39>.
- [44] B. H. Shaker. et al, "Grid Search-Based Hyperparameter Tuning and Classification of Microarray Cancer Data", *Second International Conference on Advanced Computational and Communication Paradigms (ICACCP)*, pp. 1-8, (2019) DOI: 10.1109/ICACCP.2019.8882943.